ABraytCSPfuture

Air-Brayton Cycle Concentrated Solar Power future plants via redox oxides-based structured thermochemical heat exchangers / thermal boosters

Deliverable D4.1. First version of chemical/transport processes simulation results in redox structures

Dissemination Level: Sensitive

WP4 Dual-bed prototype design and solar thermal power plant level system integration scenarios
Date: 31.10.2024

https://www.abraytcspfuture.eu/

Disclaimer

The work described in this document has been conducted within the ABraytCSPfuture project that is co-funded by the European Union. Views and opinions expressed herein are however those of the author(s) only and do not necessarily reflect those of the European Union or of the granting authority, European Climate, Infrastructure and Environment Executive Agency (CINEA). Neither the European Union nor the granting authority can be held responsible for them.

Grant Agreement Number: 101084569 Acronym: ABraytCSPfuture				
Full Title	**A**ir-**Brayt**on Cycle **C**oncentrated **S**olar **P**ower **future** plants via redox oxides-based structured thermochemical heat exchangers/thermal boosters			
Call Topic Identifier:	HORIZON-CL5-2021-D3-03			
Funding Scheme	HORIZON EUROPE, RIA – Research and Innovation Actions			
Project start date:	01.11.2022			
Project duration:	48 months			
Project URL	https://www.abraytcspfuture.eu/			
EU Project Officer	Clara Astudillo Llorente			
Project Coordinator	DLR – German Aerospace Center			
Deliverable	D4.1 – Chemical/transport processes simulation results in redox structures			
Date of Delivery	Contractual	31.10.2024	Actual	31.10.2024
Nature	Report			
Dissemination Level	Sensitive			
Lead Beneficiary	University of Twente (UT)			
Document History				

Version	**Issue Date**	**Change History**	**Authors**	**Organisation**
1.0	29.10.2024	Document drafted	Cao Zhen	UT
1.1	30.10.2024	Updated with final partner feedback	G. Karagiannakis, C. Agrafiotis	CERTH, DLR
1.2	30.10.2024	Final Review	Iñigo Muñoz	TEKN

About the Project

ABraytCSPfuture sets forth an innovative, carbon-neutral way for implementing the highly efficient air-Brayton gas turbine power generation cycles into future air-operated Concentrated Solar Power (CSP) plants. Air-Brayton cycles are used in traditional power plants where, however, involve fossil fuels combustion via pressurized air. *ABraytCSPfuture*'s carbon-neutral approach aims at achieving higher solar-to-electricity efficiencies, vital for competitiveness of CSP and non-reachable by either PVs or molten salts and thermal oils, increasing in parallel significantly the plants' storage capability. The project will develop and demonstrate a first-of-its-kind compact, dual-bed thermochemical reactor/heat exchanger unit that will transfer heat from a non-pressurised air stream to a pressurised one, while also operating as a thermal booster, raising the temperature of the pressurized stream to the level required for Brayton cycles. Furthermore, the volumetric solar energy storage density of air-operated CSP plants will be significantly increased by rendering their current sensible-only regenerative storage systems to hybrid sensible-thermochemical storage ones within the same storage volume. Both these functionalities will be materialized by thermochemical reactor/heat exchanger units comprised of non-moving, flow-through porous ceramic structures (honeycombs or foams) based on earth-abundant, cost-efficient, non-toxic oxide materials and exploiting reversible reduction/oxidation reactions of such oxides in direct contact with air, accompanied by significant endothermic/exothermic heat effects. The proposed technology is set forth by an interdisciplinary partnership spanning the entire CSP value chain, comprised of leading research centres, universities, innovative SMEs and large enterprises, including ancillary services providers and technology end-users.

Deutsches Zentrum fuer Luft- und Raumfahrt e.V., **DLR**	DE	DLR
Centre for Research & Technology Hellas, **CERTH**	EL	CERTH CENTRE FOR RESEARCH & TECHNOLOGY HELLAS
University of Twente, **UT**	NL	UNIVERSITY OF TWENTE.
Fundación CENER, **CENER**	ES	CENER NATIONAL RENEWABLE ENERGY CENTRE ADItech
Fundación TEKNIKER, **TEKN**	ES	Tekniker
Fraunhofer Gesellschaft zur Foerderung der angewandten Forschung e.V., **FHG (IWKS)**	DE	Fraunhofer IWKS
OPRA Turbines, **OPRA**	NL	Destinus
KRAFTBLOCK GmbH, **KB**	DE	KRAFT BLOCK
LANDSON Emission Technologies A/S, **LET**	DK	landson
COBRA Instalaciones y Servicios S.A., **COBRA**	ES	cobra

Table of Contents

This deliverable is part of a project that has received funding from the European Union's Horizon Europe research and innovation programme under grant agreement no 101084569

Executive Summary

The present document constitutes Deliverable D4.1 "First version of chemical/transport processes simulation results in redox structures" developed within *WP4 Dual-bed prototype design and solar thermal power plant level system integration scenarios* of the HORIZON EUROPE 2020 ABraytCSPfuture project. This document illustrates the progress of numerical simulations of the thermochemical process in honeycomb structures (porous media). The current simulation was carried out based on cobalt oxide (Co_3O_4/CoO) with known reaction kinetics and thermal properties. Through the simulation, the routine for the chemical/transport process simulations in the redox structures could be confirmed, which as a next step could be implemented for new materials, i.e., $CaMnO_3$-based perovskites (calcium-manganese-oxide) as soon as the reaction kinetics and thermal properties are identified by WP2 and WP3.

The numerical model was established, mainly considering the flow in free domains, the flow in the porous domain (honeycomb), heat transfer in the porous domain, and species transport due to the redox reaction occurring in the porous domain. The model was validated by comparison to experimental measurements (Tescari et al. 2017), concerning the available/reported solid temperature of the porous domain, and showing good agreement. The validated model was used to perform a parametric study. The variation in porosity and site species density considerably influence the reduction (charging) and oxidation (discharging) duration. Afterward, the model was upgraded by replacing the jump boundary conditions (accounting for inertial resistance) with the experimentally measured values of the Forchheimer coefficient and the Darcy permeability from DLR. This upgraded model was used to investigate the performance of honeycombs having cell densities 400 cpsi, 600 cpsi, and 900 cpsi (cells per square inch).

Changes with respect to the DoA;

No changes or Deviations from the Work plan occurred concerning this Deliverable *D4.1 Chemical/transport processes simulation results in redox structures*.

.

1. Introduction

1.1 Motivation

The project focussed on the development of a first-of-its-kind compact, dual-bed thermochemical reactor/heat exchanger unit for heat storage and temperature boosting by hybrid sensible-thermochemical heat storage. The reactor unit is composed of non-moving, flow-through porous structures (honeycombs or foams) based on earth-abundant, cost-efficient, non-toxic metal oxide materials that are in direct contact with hot air from the CSP receiver. Several chemical/transport processes are critically important to influence the performance of the reactor, e.g., the flow in the porous structure, the heat exchange between the air and the solid in the porous structure as well as heat conduction/radiation in the solid, and the redox thermochemical reaction. Numerical simulation, as a counterpart of the experimental campaign, is an important and efficient way to reveal the performance of the thermochemical reactor, e.g., the effect of porous characteristics on reaction propagation, temperature evolution, and redox time, and helps to define important operational and geometrical parameters of the porous structure, providing important insights into the design and performance of the thermochemical heat storage reactor.

Deliverable 4.1 is produced within the dual-bed prototype design and solar thermal power plant level system integration scenarios workpackage (WP4) and specifically within Task 4.1. Computational simulation of flow and heat transfer processes inside porous redox oxide media under reactive conditions, wherein partners UT, DLR, and CERTH participate. In this deliverable, a numerical model was developed based on a model redox metal oxide (Co_3O_4), as a starting point which will be further modified and developed to study the reactor with the new $CaMnO_3$-based redox materials when its thermophysical properties and reaction kinetics are available.

1.2 Literature review

Thermochemical energy storage (TCES) is a promising way for heat storage. Among different TCES technologies depending on the type of reactive materials [1], metal oxides are preferable, since they could achieve comparatively high temperatures >1000 K [2], rendering TCES a promising technology to secure renewable energy deployment, e.g., concentrated solar power (CSP) applications. Furthermore, compared to hydroxides, metal hydrides, and carbonates, no separate gas storage is needed, which could simplify the thermochemical heat storage system. Up to date, several metal oxides have been synthesized and their thermochemical performance has been experimentally explored, for example, BaO_2 by Carrilo et al. [3], Mn_2O_3 by Karagiannakis et al. [4], MgO/MnO mixture by Hayes et al. [5], La-Sr-Co-Mn and La-Sr-Co-Fe-based perovskites by Babiniec et al. [6], $SrFeO_3$ by Chen et al. [7], $CaMnO_3$ foam by Pein et al. [8]. Most available measurements are limited to a TGA scale, while Agrafiotis et al. [9] demonstrated a lab-scale reactor of Co_3O_4-coated and Mn_2O_3-coated foams and honeycombs, and Tescari et

al. [10] scaled it up to a pilot-level study. Perovskites and in particular $CaMnO_3$-based ones constitute a promising family of redox compositions as they can be abundant, cost-effective and their redox behaviour is well documented. Moreover, contrary to simple metal oxides such as manganese and cobalt ones, their cyclic redox function is free of any major phase changes which are known to be potentially detrimental to thermo-mechanical stability of structured building blocks of candidate TCES reactors.

In addition to the experimental studies, numerical simulations have been developed to design and reveal the thermochemical reactor performance. The numerical study is cost-effective, but it is not easy to establish a convincing model because of its complexity in multiple transport processes (flow, heat transfer, and species transport). For example, in a thermochemical reactor having porous structures, the heat transfer mechanism in the porous domain includes interstitial convection (local thermal non-equilibrium), heat conduction, and heat radiation at high temperatures, while reaction kinetics need to be correctly modelled for species transport (typically oxygen for redox schemes). Wu et al. [11] numerically investigated ceramic foam-based volumetric solar air receivers. The pressure drop in the ceramic foams and the interfacial heat transfer between the flowing fluid and solid were included in the model, while the radiative heat transfers due to concentrated solar radiation absorption by the ceramic foam and the radiation transport in the media were modelled using the P_1 approximation. The results illustrated that the thermal non-equilibrium phenomena were locally important. Tescari et al. [12] numerically studied a solar rotary kiln as a high-temperature thermochemical reactor. However, still, they only considered coupled flow and heat transfer in the reactor, without species transport. Similar simulations were also available for a lab-scale particle-packed thermochemical reactor [13]. Later, Singh et al. [14] comprehensively modelled honeycomb-structure reactors based on the Co_3O_4/CoO looping cycle, considering the fluid flow and heat transfer (interstitial convection (thermal non-equilibrium), heat conduction/radiation, and reaction enthalpy) in the honeycomb and the chemical reaction, followed by several similar simulations [15, 16]. In comparison, some work assumed thermal equilibrium state between the fluid and porous matrix in the reactor, e.g., the reduction of iron–manganese oxide particles in a lab-scale packed-bed reactor [17]. Recently, Korba et al [18, 19] developed continuum models for heat and mass transfer in moving-bed reactors of magnesium-manganese-oxide particles, considering both the gas and particle phases at the continuum scale and to be in hydraulic/thermal non-equilibrium. The reaction kinetics are coupled with mass, momentum, species, and heat transfer to describe transport phenomena within the reactor.

The above literature shows the advance in numerical simulations of different types of thermochemical reactors, indicating the key processes that need to be considered. Concerning the reactor of non-moving, flow-through porous structures (honeycombs or foams), the crucial process includes fluid flow and heat transfer in the porous structure, species transport, and reaction kinetics. Although a few simulations have been performed, there is room for improvement, e.g., via the flow simulation in porous media, and the heat transfer modelling in the porous structures. In addition, parametric studies are required

to consolidate the understanding of the reactor performance and provide insights into reactor design.

1.3 Content of this report

The report summarizes the activities and results relevant to the simulation of chemical/transport processes in redox structures of honeycombs. Firstly, a numerical model was proposed based on the Co_3O_4/CoO model system, involving the physical process of flow in both free and porous domains, internal heat transfer in the porous domain (interstitial convection, heat conduction, heat radiation, and reaction enthalpy), species transport, and reaction kinetics.

- The detailed geometry of a honeycomb, which is rather computationally heavy, was not considered for this first version of the simulation. Instead, a domain was defined with a certain value of porosity to mimic the honeycomb characteristics, and the flow in the porous media was simulated by considering a Darcy permeability to account for the viscous resistance and using a jump boundary condition to account for the inertial resistance. The Darcy permeability and the Forchheimer coefficient were estimated by Darcy's law and flow contraction (honeycomb inlet)/expansion (honeycomb outlet), respectively.
- The heat radiation was implicitly simulated, by adding an equivalent thermal conductivity to the thermal conductivity of the redox material.
- A user-defined reaction rate was provided to simulate the redox phenomena, which depends on the extent of the reaction and the reaction rate constant defined by the Arrhenius equation.

The model was validated with the available experimental measurements from DLR, and then the parametric study was performed to investigate the effect of porosity and site species density variation on the redox process. Afterwards, the flow simulation in the porous domain was improved by including the measured values of Darcy permeability and Forchheimer coefficient from DLR, and the redox performance was further investigated for the three honeycomb densities (400 cpsi, 600 cpsi, and 900 cpsi).

2. The numerical model

2.1 Reactor geometry and simulation domain

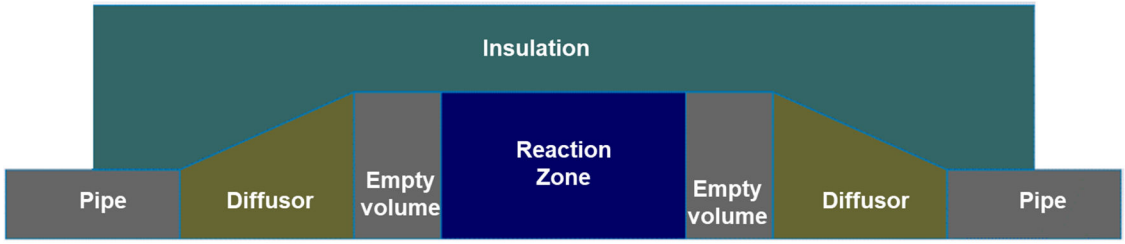

Figure 1: The simulation domain (reactor geometry).

The reactor configuration is shown in Figure 1. It consists of a chamber with cordierite honeycombs inside, while the honeycomb is coated with the reactive material (Co_3O_4). Hot air from the volumetric solar receiver is supposed to flow through an inlet pipe, a diffusor, an empty volume, and enter into the reaction zone where the honeycomb is positioned. Subsequently, the air exits the reactor system through a diffusor; i.e. an empty volume.

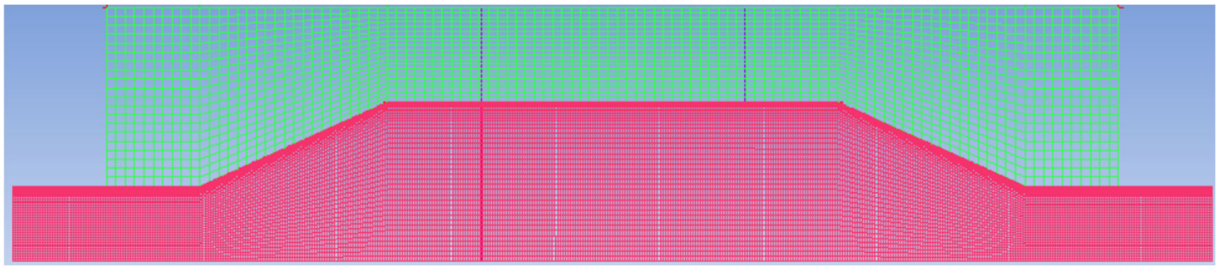

Figure 2: Grid system of the simulation domain.

The simulation domain was created using SolidWorks, while ICEM was used to generate the mesh as shown in Figure 2. In the insulation domain, the mesh has a large size of 8-20 mm, while the mesh in the other domains is much more refined to resolve flow and heat transfer, for example the mesh size of the first layer on the reaction zone wall is 0.6 mm. The total cell number is 30618. The selected mesh resolution allows obtaining grid-independent results.

2.2 Thermal properties of the involved materials

The materials involved in the simulation include cobalt oxide (Co_3O_4 in discharge state and CoO in charged state), cordierite, and thermal insulation materials (Insulfrax and Promat). The thermal properties are summarized in Table 1 as shown below. The heat capacity and thermal conductivity are temperature-dependent.

Material	C_p (J/kg·K)	ρ (kg/m3)	λ (W/m·K)
Co_3O_4	$0.55T + 328.6$	6110	$-1.25\cdot10^{-8}\ T^3 + 4.27\cdot10^{-5}\ T^2 - 5.78\cdot10^{-2}\ T + 33.381$
CoO	$0.12T + 628$	6450	-
Cordierite	$5\cdot10^{-7}\ T^3 - 1.9\cdot10^{-3}\ T^2 + 2.3033\ T + 664.18$	2000	2.5
Insulfrax	1000	2670	$4\cdot10^{-4}\ T - 0.1406$
Promat	$-3.75\cdot10^{-2}\ T^2 + 9.296\ T + 503.99$	280	$1.875\cdot10^{-8}\ T^2 - 7.48\cdot10^{-6}\ T + 0.024$

Table 1: Thermal properties of the involved materials [14].

2.3 The model description

The critical concern is the simulation of the redox reaction in the porous domain. Therefore, the flow model, heat transfer model, transport species, and reaction kinetics in the porous domain will be detailed in this section. The redox reaction is shown as

$$Co_3O_4 \leftrightarrow 3CoO + 1/2O_2 \quad (1)$$

Flow model

In the porous domain, the mass conservation equation takes into account the porosity, ϕ, and can be expressed as:

$$\frac{\partial}{\partial t}(\phi\rho) + \nabla \cdot (\phi\rho\vec{u}) = R_m \quad (2)$$

ϕ: Porosity of the medium (fraction of void space),

ρ: Density of the fluid within the porous domain,

R_m: Source term representing mass change due to redox reactions of the metal oxide.

The momentum equation for the fluid phase in the porous domain, without assuming Darcy's law, can be written as

$$\frac{\partial}{\partial t}(\phi\rho\vec{u}) + \nabla \cdot (\phi\rho\vec{u}\vec{u}) = -\phi\nabla P + \nabla \cdot (\phi\mu\nabla\vec{u}) + \phi\rho\vec{g} - \frac{\mu}{\kappa}\vec{u} - \beta\rho|\vec{u}|\vec{u} \quad (3)$$

μ: Dynamic viscosity of the fluid,

κ: Permeability of the porous medium, representing the viscous resistance,

β: Forchheimer coefficient, accounting for the inertial resistance.

Heat transfer model

In the porous domain, a thermal non-equilibrium state is considered between the fluid and the porous matrix. Thus, the energy equation of both fluid and solid needs to be solved. Several heat transfer mechanisms inside porous media are considered, including the interstitial heat transfer between the fluid and solid, heat conduction in the fluid and solid, heat radiation in the solid, and reaction enthalpy.

The energy equation of the fluid phase is formulated as

$$\frac{\partial}{\partial t}\left(\phi\rho_f C_{p,f} T_f\right) + \nabla \cdot \left(\phi\rho_f C_{p,f} T_f \vec{u}\right) = \nabla \cdot \left(\phi k_f \nabla T_f\right) + h_{sf} A\left(T_s - T_f\right) + Q_{rxn,f} \quad (4)$$

The energy equation of the fluid phase is formulated as

$$(1-\phi)\frac{\partial}{\partial t}\left(\rho_s C_{p,s} T_s\right) = \nabla \cdot \left((1-\phi) k_s \nabla T_s\right) + h_{sf} A\left(T_f - T_s\right) + Q_{rxn,s} \quad (5)$$

h_{sf}: Interstitial heat transfer coefficient in porous media,

Q_{rxn}: Heat generated or released due to the redox reaction.

It is worth mentioning that the solid thermal conductivity in Eq.(5) is not equal to the value of cordierite in Table 1, because the value in Table 1 does not correspond to the honeycomb monolith. Visconti et al. [20] developed a simple model for the accurate prediction of the thermal conductivity of honeycomb monoliths with square channels in axial and radial direction, which depends on the thermal conductivity of the solid material and the porosity of the honeycomb.

The effective thermal conductivity in flow direction is described as

$$\lambda_{s,a} = \lambda_{Cordierite}(1-\phi) \quad (6)$$

The effective thermal conductivity in radial direction (or direction perpendicular to the flow direction) is described as

$$\lambda_{s,r} = \lambda_{Cordierite} \frac{(1-\phi)}{1+\phi} \quad (7)$$

Therefore, the solid thermal conductivity in Eq. (5) is an orthotropic conductivity.

In addition, heat radiation in the solid is not explicitly modelled. Instead, an equivalent thermal conductivity is added to the solid thermal conductivity in Eq. (5) to account for the heat radiation. This way to model heat radiation is extensively employed in the literature [14, 19]. The detailed process to derive this equivalent thermal conductivity is reported by Lantin [21]. Concerning the temperature range in this report, the equivalent thermal conductivity is expressed as

$$\lambda_{rad} = 1.3549 \cdot 10^{-6} T^2 - 2.161 \cdot 10^{-3} T + 0.8916 \quad (8)$$

This radiative conductivity is also added to the solid thermal conductivity in Eq. (5).

Species transport

During the redox reaction, Co_3O_4 is reduced to CoO and O_2. Since ANSYS Fluent does not support the consumption and formation of solid material, Co_3O_4 and CoO are regarded as site species that are deposited on the surface of the porous domain, while gaseous O_2 could be consumed and generated, which can be described by the species transport equation as

$$\frac{\partial}{\partial t}(\phi \rho_f C) + \nabla \cdot (\phi \rho_f C \vec{u}) = \nabla \cdot (\phi D_{eff} \nabla C) + R_C \quad (9)$$

C: Concentration of species

D_{eff}: Effective diffusivity of species C

R_C: Source term for species C, the production or consumption rate due to redox reactions. In this case, the source term R_C represents the net volumetric rate of oxygen, R_{O2} which can be coupled with the reaction rate of Co_3O_4 with the stoichiometric coefficient: $R_{O2} = R_{Co3O4}$.

Reaction kinetics

The reaction rate of the Co_3O_4 /CoO pair is defined in a previous study [22], as

$$R_{Co3O4} = k_1(1 - X) - k_2 X \quad (10)$$

k_1 and k_2 c ould be calculated by the Arrhenius equation, as

$$k_1 = 2.12 \times 10^{27} \cdot e^{\frac{-8200}{T}} \quad (11)$$

$$k_2 = 1.4 \times 10^{-15} \cdot e^{\frac{30000}{T}} \quad (12)$$

X is the conversion of Co_3O_4 defined by

$$X = 1 - \frac{n_{Co3O4}}{n_{Co3O4,o}} \quad (13)$$

n_{Co3O4} is the instant site density of Co_3O_4, $n_{Co3O4,0}$ is the initial site density of Co_3O_4.

2.4 Boundary conditions

Figure 1 shows the simulation domain. It is also seen that the boundary conditions mainly include inlet and outlet boundary conditions, wall boundary conditions of the insulation zone, and the interface between the insulation domain and the porous domain.

- At the inlet boundary condition, the velocity and temperature were defined as a velocity profile and a temperature profile, respectively, which were obtained from the measurement [14]. The mass fraction of oxygen at the inlet was assumed as 0.232.
- At the wall boundary conditions, mixed thermal conditions were used, representing heat losses from the insulation wall to the surroundings by natural convection and heat radiation.
- In the porous domain, insulation was thermally coupled only with the solid cells while the interface between fluid cells and insulation was assumed to be adiabatic.
- Porous jump boundary conditions can be used to estimate the viscous and inertial resistance in honeycombs with square channels. These conditions were only used when the experimentally determined values of Darcy permeability and the Forchheimer coefficient were not available.

3. Results and discussion

This section demonstrates the results of the numerical simulation. First, the model was validated against the available experimental results from the literature [Tescari et. al 2017]. Afterwards, the validated model was used to study the effect of porosity and site density of species on the redox reaction process. Finally, the flow model was modified by using experimentally measured Darcy permeability and the Forchheimer coefficient, and the redox performance in different honeycombs was again investigated by the modified model.

3.1 Model validation

The transient solid temperature profile on representative functional parts of the porous domain like the point of inlet and the middle (as shown in the insert in Figure 3) was extracted from the simulation, which was then compared with the experimental measurement, as shown in Figure 3. It is seen that the simulation result agrees well with the experimental result, indicating that the model is reliable.

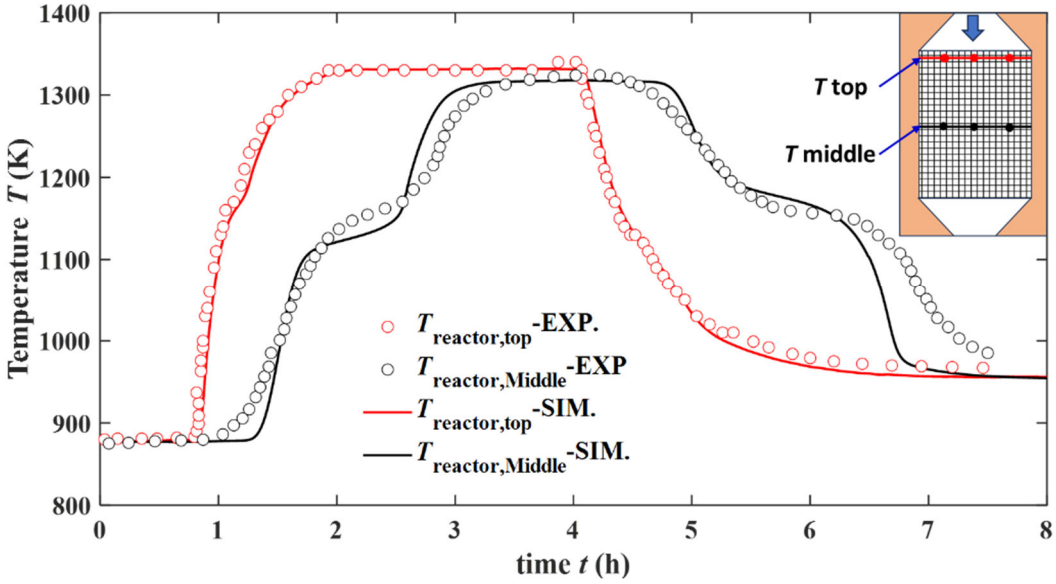

Figure 3: Comparison of the solid temperature between the model and the experiment during a redox cycle.

The solid temperature is considerably affected by the incoming air temperature. At the beginning of the charging process, the solid material is heated by the incoming hot air, indicating quick temperature increase. When the solid material temperature reaches around 1170 K, the temperature profile becomes flat, indicating the occurrence of the reduction reaction which absorbs the heat from the incoming hot air. When the reduction completes at around 3 h, the temperature starts to increase quickly again because the incoming air has a high temperature of around 1350 K between 3 h and 4 h which can continue heating the solid material. From 4 h, the temperature of the incoming air quickly decreases to around 973 K, and then the solid material is cooled down. The oxidation reaction is observed at around 5.5 h. During the oxidation, the air is heated up by the energy of the exothermic oxidation reaction, and the solid temperature decreases relatively slowly. When the oxidation is finished at around 6.5 h, the solid material is quickly cooled down by the, at that time, colder air flow.

3.2 Reaction propagation

The numerical simulation enables us to dive into details of the reaction progress in the porous domain. Since the redox reaction considerably affects the temperature, the temperature field is compared at different times, corresponding to different states of the material and chemical reaction status, as shown in Figure 4. In the period when the redox material is heated (0-4h), it is seen that this heating takes place in a stratified manner; i.e. from the inlet and gradually to the outlet, and the central part is heated up faster compared to the side part, generating a parabolic temperature front. In the period when the redox material is cooled (4-8h), the temperature profiles show some similar characteristics to those during the heating period. For example, the cooling also starts from the inlet and gradually develops into the outlet. Compared to the heating period, the cooling rate is almost the same between the central part and the side part, exhibiting an almost horizontal temperature front.

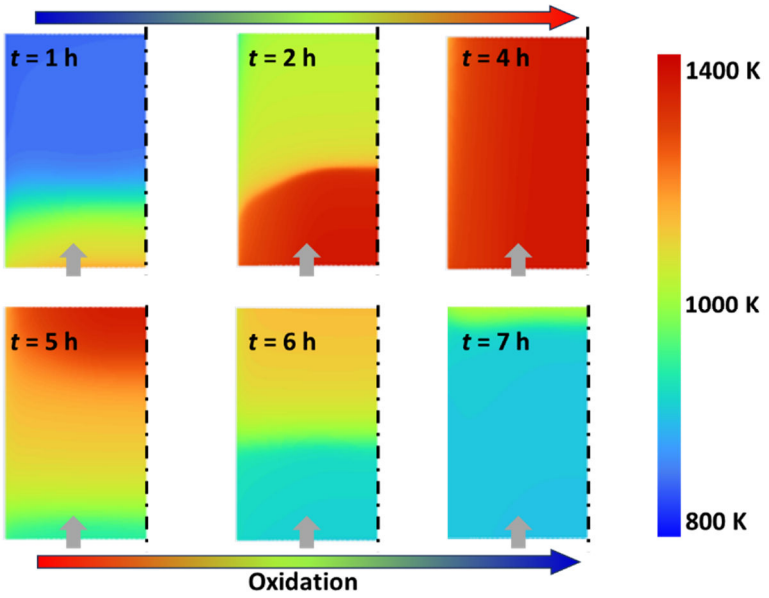

Figure 4: Temperature evolution of the redox material inside the reactor.

Figure 5 describes the change of Co_3O_4 site density over time, indicating the (reduction/charging) reaction propagation. It is shown that the reaction advancement is consistent with the temperature evolution. For example, in the reduction process, the reaction advance also has a parabolic profile. The reaction starts from the inlet where the temperature is high and completes quickly in the region with high temperature.

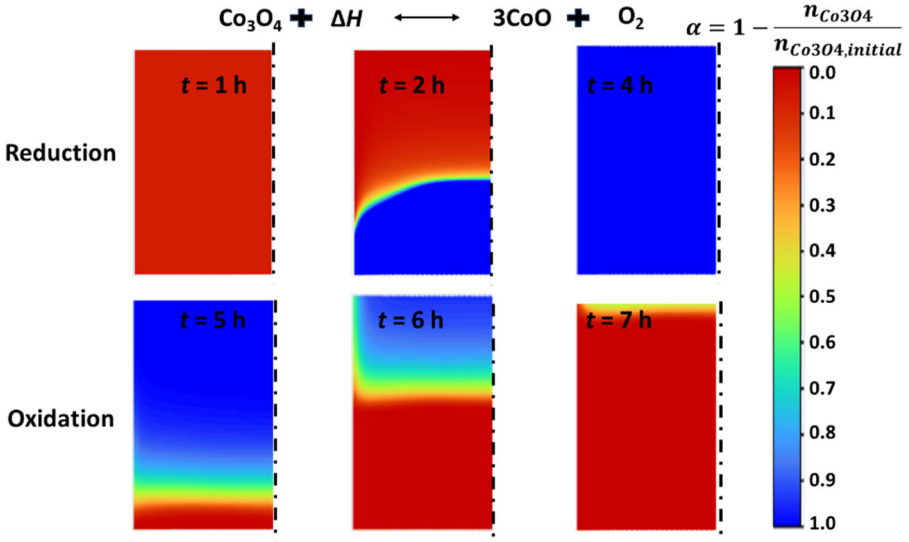

Figure 5: The reaction advancement with time.

3.3 Parametric study

The validated model reveals a strong connection between the redox reaction and the redox material temperature. In this section, the effects of variation of porous domain porosity and of the site density of the redox material are investigated. When changing the porosity, the wall thickness of honeycomb channels is assumed to be constant (0.37 mm), and only the channel width changes as 0.57 mm (porosity 0.443), 1.51 mm (porosity 0.687), and 3.39 mm (porosity 0.835), respectively.

Figure 6 compares the temperature profile vs. time in the middle of the porous domain for three different porosity values. It is seen that the temperature starts to increase and decrease earlier with a higher porosity. It can be also roughly recognized that the temperature changes quickly (increase in the charging process and decrease in the discharging process) with the high porosity. If we visit the energy equation (5) which controls the solid temperature in the porous domain, the temperature change is due to the contribution of thermal conduction, interstitial heat convection, and reaction enthalpy. To intuitively and simply understand the reason behind this temperature performance shown in Figure 6, we take the initial charging process before reaching the reduction as an example, and we further neglect the thermal conduction inside the solid because the conductive thermal resistance could be much smaller than thermal resistance of interfacial convection for cordierite. Then, it is clear that high porosity and high interfacial heat transfer (high interstitial heat transfer coefficient and large specific area) bring out quick temperature change against time.

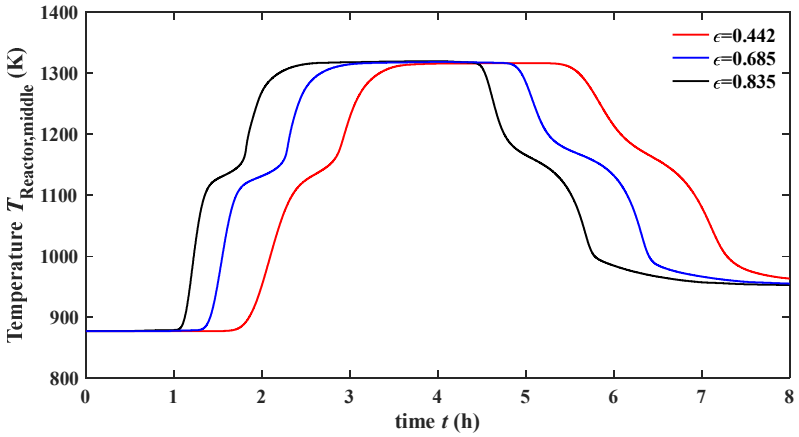

Figure 6: Comparison of the temperature profiles in the middle of the porous domain with varying porosity.

The site density of Co_3O_4 represents the amount of the available redox material which is considered to affect the amount of the total energy stored. We varied the site density from 2.76 mol/m^2 to 7.11 mol/m^2 while keeping the porosity at a constant value of 0.685. The temperature in the middle of the porous domain is again compared, as shown in Figure 7. It is seen that this parameter does not affect the initial sensible heat storage in the charging process, but the reduction completes within a shorter time in the case of a low site density. Therefore, and as expected, less site density decreases the amount of thermochemical heat. Similarly, in the discharging process the site density does not affect the sensible cooling. Starting from the oxidation occurrence at around 5h, the temperature profile becomes divergent, indicating that the high site density could provide a high-temperature output because it stores a large amount of heat in the charging process.

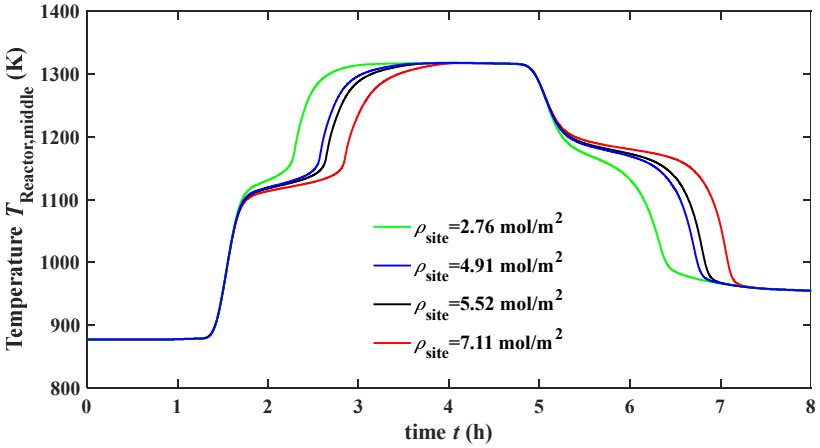

Figure 7: The comparison of the temperature in the middle of the porous domain with various site density of Co_3O_4.

3.4 Simulation of honeycombs measured by DLR

DLR established a setup to measure Darcy permeability and Forchheimer coefficient of porous media. Three cordierite honeycombs with no redox oxide material coated on them have been measured, as shown in Table 2.

cpsi (cells per square inch)	wall thickness (m)	channel width (m)	porosity	Darcy permeability (m^2)	Forchheimer coefficient (m^{-1})
400	0.0001	0.0011684	0.8464	4.47E-08	22.88
600	0.0001	0.0009354	0.8136	3.11E-08	50.76
900	0.00005	0.0007959	0.8836	2.78E-08	74.07

Table 2: Measured Darcy permeability and Forchheimer coefficient values for 3 different honeycomb geometries.

In this simulation, we used the measured permeability and Forchheimer coefficient values to account for the viscous resistance and the inertial resistance in the honeycomb, respectively. Figure 8 compares the pressure drop of the flow in the honeycomb of 400 cpsi between the numerical results and the experimental results, which shows very good agreement. Thus, the flow can be accurately modelled with the critical input from the measurement. In this case, the jump boundary condition is not needed.

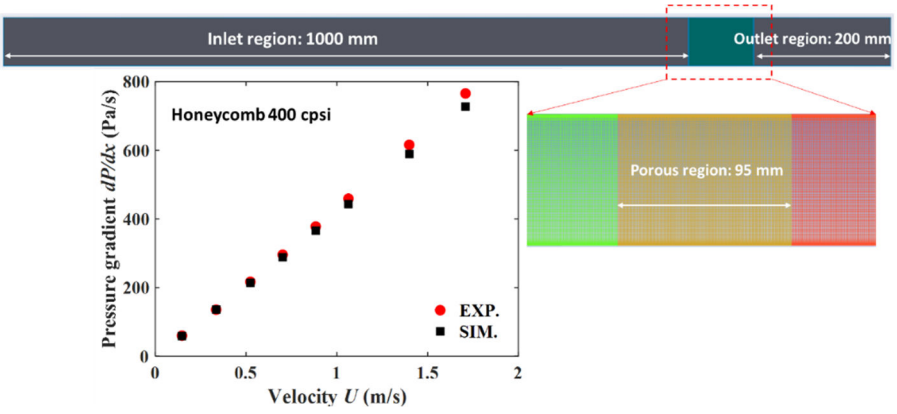

Figure 8: Flow simulation in the honeycomb of 400 cpsi.

Then, the thermochemical performance was simulated with the honeycomb of 400 cpsi. Figure 9 compares the honeycomb temperature changing against time at the inlet, middle, and outlet of the reactor. It can be seen that the redox reaction occurs earliest at the inlet of the reactor, because the inlet region is first heated in the charging process and cooled in the discharging process.

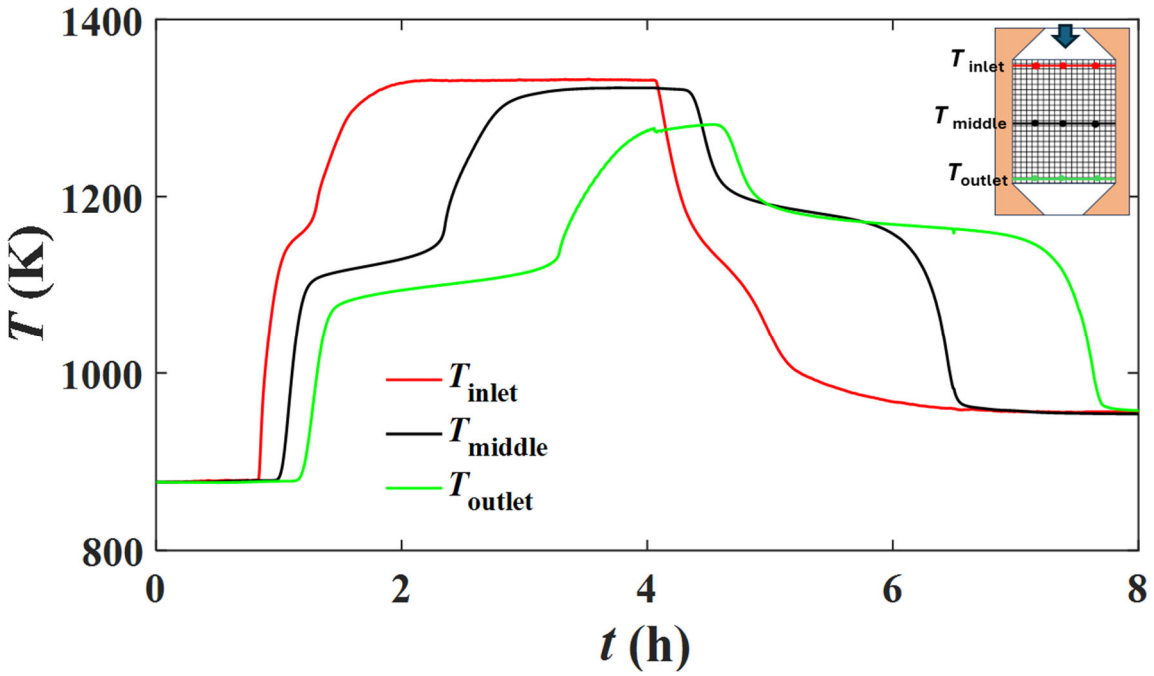

Figure 9: The temperature at the inlet, middle and outlet of the reactor (400 cpsi).

As discussed earlier, the reaction evolution strongly depends on the honeycomb temperature characteristics. Then, the overall honeycomb temperature field could indicate the reaction dynamics more intuitively. Figure 10 shows the honeycomb temperature field changing vs. time which has very similar characteristics to that in Figure 4. The inlet region is firstly heated up and cooled down in the charging process and in the discharging process, respectively.

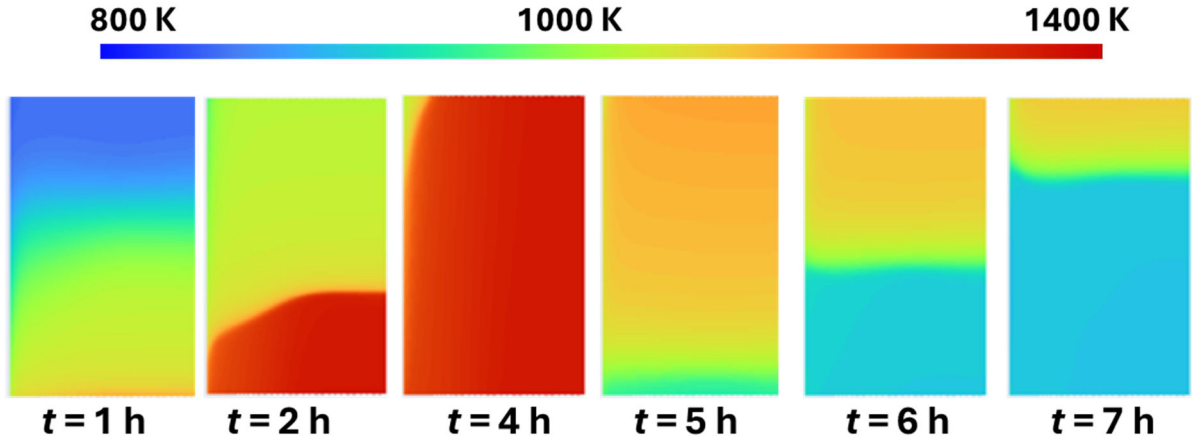

Figure 10: The honeycomb temperature evolution against time (400 cpsi).

Figure 11 compares the temperature profile of the three honeycombs which have different porosity. It is interesting to see that in the charging process, the honeycomb of

900 cpsi has slightly faster sensible heating. When it comes to the reduction reaction indicated by the plateau phase in the charging process, the honeycomb of 900 cpsi has a longer reduction duration. The same applies to the discharging (oxidation) process, which is preferable in practical applications.

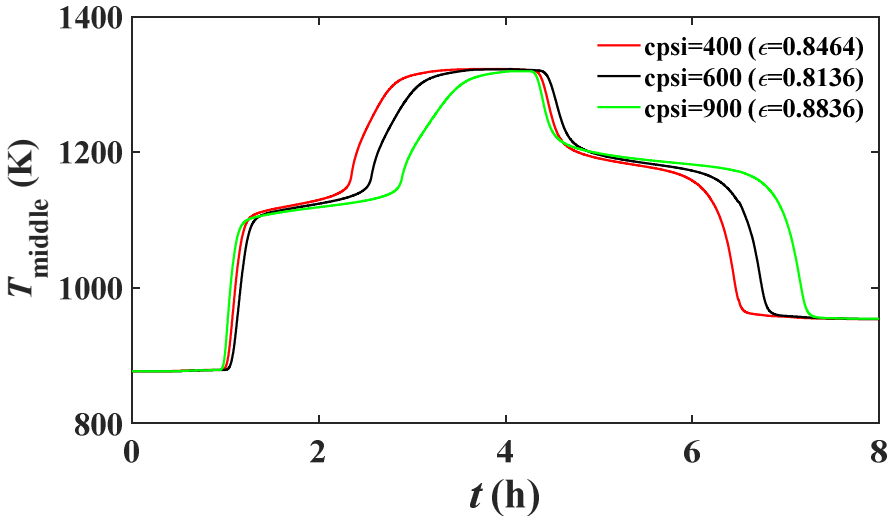

Figure 11: Comparison of temperature in the middle of various honeycombs.

A detailed comparison between Figure 11 and Figure 6 concerning the study of porosity, reveals not only some consistent findings but also some differences. In Figure 6, the porosity is free-defined by simply changing the honeycomb channel width and keeping the channel wall thickness constant, which is like the cases of 400 cpsi and 600 cpsi in Figure 11. In general, the 400 cpsi and 600 cpsi show similar effects on the temperature performance as those in Figure 6, indicating that the high porosity has short charging and discharging durations. In contrast, 900 cpsi (wall thickness different from 400 cpsi and 600 cpsi) has the highest porosity in Fgirue11, which however demonstrates the longest charging/discharging process. Therefore, when designing honeycombs, the same porosity could be achieved with different designs of honeycomb channel dimensions (channel width and wall thickness). We not only consider the value of porosity but also need to consider the dimension and layout of the honeycomb channel. The effect of honeycombs on the thermochemical reactor performance is a comprehensive result of many coupled parameters, including porosity, flow condition, specific surface area, etc.

Conclusions

This deliverable provides the first version of the chemical/transport process in redox structures. The flow in the porous structure, the chemical reaction, and heat transfer in the porous structure are essentially important to implement the simulation convincingly.

- Numerical models have been developed to investigate the performance of thermochemical reactors, and the model was validated by experimental data available in the relevant literature.
- The model reveals the characteristics of the reaction propagation. The reaction starts at the reactor inlet and gradually evolves to the reactor outlet. In the charging process, the reaction proceeds faster in the central part than in the side part.
- Preliminary results are achieved, concerning the parametric study of porosity and site species density. A high site density could increase the amount of charged heat and provide higher temperature output at the discharging process.
- The measurement of Darcy permeability and Forchheimer coefficient helps to improve the flow simulation in the porous domain.
- Concerning three honeycomb geometries with measured permeability and Forchheimer coefficients, numerical simulations were carried out to assess the thermochemical reactor performance as a function of the cells density. The honeycomb of 900 cpsi demonstrated a longer reduction and oxidation duration.

Future activities

The present work sets up a convincing numerical routine to model thermochemical reactors based on redox reactions. The following activities will mainly include two parts.

[1] We will work on the geometric design of the porous structures in the reactor, based on the currently developed model. Specifically, we will develop codes of user-defined-functions (UDFs) in ANSYS to flexibly define local porous characteristics (porosity, Darcy permeability, Forchheimer coefficient, interstitial heat transfer coefficient, specific surface area, etc.) in the porous domain. With the UDFs, we aim to study the flow performance and the thermochemical performance of various layouts of porous structures, and then provide guidelines on the design of the porous structures, e.g., the porosity distribution along the flow and radial directions.

[2] Through this deliverable, we obtain experience and insights into constructing convincing numerical models for the thermochemical reactor. The current model could be further modified and developed to study the reactor with new redox materials, with strong support and collaboration from WP2 and WP3.

References

[1] Yan Y, Wang K, Clough PT, Anthony EJ. Developments in calcium/chemical looping and metal oxide redox cycles for high-temperature thermochemical energy storage: A review. Fuel Processing Technology. 2020;199.

[2] Zhao J, Korba D, Mishra A, Klausner J, Randhir K, AuYeung N, et al. Particle-based high-temperature thermochemical energy storage reactors. Progress in Energy and Combustion Science. 2024;102.

[3] Carrillo AJ, Sastre D, Serrano DP, Pizarro P, Coronado JM. Revisiting the BaO2/BaO redox cycle for solar thermochemical energy storage. Phys Chem Chem Phys. 2016;18(11):8039-48.

[4] Karagiannakis G, Pagkoura C, Zygogianni A, Lorentzou S, Konstandopoulos AG. Monolithic Ceramic Redox Materials for Thermochemical Heat Storage Applications in CSP Plants. Energy Procedia. 2014;49:820-9.

[5] Hayes M, Korba D, Schimmels P, Klausner J, Petrasch J, AuYeung N, et al. Experimental demonstration of high-temperature (>1000 °C) heat extraction from a moving-bed oxidation reactor for thermochemical energy storage. Applied Energy. 2023;349.

[6] Babiniec SM, Coker EN, Miller JE, Ambrosini A. Investigation of La Sr1−Co M1−O3− (M = Mn, Fe) perovskite materials as thermochemical energy storage media. Solar Energy. 2015;118:451-9.

[7] Chen X, Kubota M, Yamashita S, Kita H. Investigation of Sr-based perovskites for redox-type thermochemical energy storage media at medium-high temperature. Journal of Energy Storage. 2021;38.

[8] Pein M, Matzel L, de Oliveira L, Alkan G, Francke A, Mechnich P, et al. Reticulated Porous Perovskite Structures for Thermochemical Solar Energy Storage. Advanced Energy Materials. 2022;12(10).

[9] Agrafiotis C, Becker A, Roeb M, Sattler C. Exploitation of thermochemical cycles based on solid oxide redox systems for thermochemical storage of solar heat. Part 5: Testing of porous ceramic honeycomb and foam cascades based on cobalt and manganese oxides for hybrid sensible/thermochemical heat storage. Solar Energy. 2016;139:676-94.

[10] Tescari S, Singh A, Agrafiotis C, de Oliveira L, Breuer S, Schlögl-Knothe B, et al. Experimental evaluation of a pilot-scale thermochemical storage system for a concentrated solar power plant. Applied Energy. 2017;189:66-75.

[11] Zhiyong Wu ZW. Coupled radiation and flow modeling in ceramic foam. Solar Energy. 2011;85.

[12] Tescari S, Neises M, de Oliveira L, Roeb M, Sattler C, Neveu P. Thermal model for the optimization of a solar rotary kiln to be used as high temperature thermochemical reactor. Solar Energy. 2013;95:279-89.

[13] de Miguel SÁ, Bellan S, de María JMG, González-Aguilar J, Romero M. Numerical modelling of a 100-Wh lab-scale thermochemical heat storage system for concentrating solar power plants. 2016.

[14] Singh A, Tescari S, Lantin G, Agrafiotis C, Roeb M, Sattler C. Solar thermochemical heat storage via the Co3O4/CoO looping cycle: Storage reactor modelling and experimental validation. Solar Energy. 2017;144:453-65.

[15] Zhou X, Mahmood M, Chen J, Yang T, Xiao G, Ferrari ML. Validated model of thermochemical energy storage based on cobalt oxides. Applied Thermal Engineering. 2019;159.

[16] Ebadi M, Mehrpooya M, Kani AH. Sensitivity analysis and optimization of geometric and operational parameters in a thermochemical heat storage redox reactor used for concentrated solar power plants. Journal of Thermal Analysis and Calorimetry. 2021;147(11):6415-35.

[17] Hamidi M, Wheeler VM, Gao X, Pye J, Catchpole K, Weimer AW. Reduction of iron–manganese oxide particles in a lab-scale packed-bed reactor for thermochemical energy storage. Chemical Engineering Science. 2020;221.

[18] Korba D, Huang W, Randhir K, Petrasch J, Klausner J, AuYeung N, et al. A continuum model for heat and mass transfer in moving-bed reactors for thermochemical energy storage. Applied Energy. 2022;313.

[19] Korba D, Hayes M, Schimmels P, Randhir K, Klausner J, AuYeung N, et al. Continuum modeling of high-temperature (>1000 °C) heat extraction from a moving-bed oxidation reactor for thermochemical energy storage. Journal of Energy Storage. 2024;82.

[20] Visconti CG, Groppi G, Tronconi E. Accurate prediction of the effective radial conductivity of highly conductive honeycomb monoliths with square channels. Chemical Engineering Journal. 2013;223:224-30.

[21] Lantin G, Numerical Investigation of Heat and Reaction Propagation in a Thermochemical Heat Storage for Concentrated Solar Power Applications, Master Thesis, 2014. TU Eindhoven, the Netherlands.

[22] Pagkoura C, Karagiannakis G, Zygogianni A, Lorentzou S, Kostoglou M, Konstandopoulos AG, et al. Cobalt oxide based structured bodies as redox thermochemical heat storage medium for future CSP plants. Solar Energy. 2014;108:146-63.